J. Chem. Sci. (2022)134:23
https://doi.org/10.1007/s12039-021-02004-2
© Indian Academy of Sciences

REGULAR ARTICLE

Ruthenium, rhodium and iridium complexes containing diazafluorene derivative ligands: synthesis and biological studies

CARLEY GIFFERT L NONGPIUR[a], DEEPAK KUMAR TRIPATHI[b], KRISHNA MOHAN POLURI[b], HEMANT RAWAT[c] and MOHAN RAO KOLLIPARA[a,*]
[a]Centre for Advanced Studies in Chemistry, North-Eastern Hill University, Shillong 793 022, India
[b]Department of Biotechnology and Centre for Nanotechnology, Indian Institute of Technology Roorkee, Roorkee 247 667, India
[c]Central Ayurveda Research Institute, Jhansi 284003, India
E-mail: mohanrao59@gmail.com

MS received 14 July 2021; revised 14 September 2021; accepted 15 September 2021

Abstract. Reaction of $[(arene)MCl_2]_2$ with bidentate 4, 5-diazafluorene-9-one (dafo) and derived Schiff-base ligands (**L1–L3**) in the presence of ammonium hexafluorophosphate yielded mononuclear cationic complexes having general formula $[(arene)MLCl]PF_6$ {M = Ru, arene = benzene (**1**, **5**, **9**); M = Ru, arene = *p*-cymene (**4**, **8**); M = Rh, arene = Cp* (**2**, **6**, **10**); M = Ir, arene = Cp* (**3**, **7**, **11**); L = 4, 5-diazafluorene-9-one (**L1**), N-(4, 5-diazafluoren-9-ylidene)aniline (**L2**), N-(4, 5-diazafluoren-9-ylidene)phenyl hydrazine (**L3**)}. All these complexes were isolated as hexafluorophosphate salts and characterized by spectral and analytical techniques such as FT-IR, UV-vis, NMR spectroscopy and ESI-Mass spectrometry. Complexes **1-3** were characterized by X-ray crystallographic studies, which indicated NN′ bidentate coordination of the ligands through pyridine nitrogen atoms of the ligand. To evaluate the biological properties of these complexes, antibacterial and antioxidant experiments have been carried out. The complexes **8**, **9** and **11** exhibited antibacterial activity against Gram-positive bacteria. Results also show that the compounds possess prominent antioxidant activity against DPPH radicals.

Keywords. Rhodium; iridium; 4,5 diazafluorene-9-one; antibacterial; antioxidant.

1. Introduction

To date, antibiotics have saved millions of lives worldwide.[1–6] Nowadays, however, many contagious diseases have failed to respond to antibiotics, rendering them ineffective and useless. This phenomenon known as antimicrobial resistance (AMR) has become one of the most significant challenges of modern medicine in the 21st century.[7–9] Antimicrobial resistance is responsible for 7,000,000 deaths every year around the world. The indiscriminate use and misuse of antibiotics by humans and irresponsible use in agriculture, animal health, and fisheries are some reasons for AMR, making it a manufactured disaster. This fact has triggered researchers to explore and search for new and modified medicines which can be used as antimicrobials. In this search, the organometallic compounds have been shown to have great potentials to be developed as new classes of antibacterial agents. For instance, half-sandwich ruthenium(II) complex $[(\eta^6\text{-arene})RuX(C_5H_4N\text{-}2\text{-}CH{=}N\text{-}Ar)]^+$, where arene = p-cymene or $C_6H_5\text{-}OCH_2CH_2OH$ and X = I, Br, or Cl have demonstrated good potential abilities to inhibit the growth of Gram-negative and Gram-positive bacteria and showed promising activity against methicillin-resistant *Staphylococcus aureus* (MRSA).[10] On another note, excess amounts of free radicals are harmful in humans because of their reactivity. The steady increase of free radicals in cells creates the conditions for so-called oxidative stress, wherein free radicals oxidize blood vessel walls, proteins, DNA and lipids. Oxidative stress can lead to various diseases, including cancer, diabetes, cardiovascular diseases, Alzheimer's disease

*For correspondence
Supplementary Information: The online version contains supplementary material available at https://doi.org/10.1007/s12039-021-02004-2.

Published online: 05 February 2022

and age-related muscular degeneration.[11] In this regard, metal complexes of ruthenium have also shown to be efficient antioxidants by reacting with free radicals.[12]

Schiff-bases containing various heterocycles are an important class of compounds with a wide range of biological applications such as antibacterial, antioxidant, antitumor, and antiviral activities.[13–15] Nitrogen-containing heterocycles such as 1,10-phenanthroline (phen.), 1,10-phenanthroline-5,6-dione and 2,2′-bipyridine are powerful N, N bidentate metal chelators. Ruthenium polypyridyl complexes derived from these ligands have been extensively studied. These complexes possess potent antibacterial activity towards Gram-positive and Gram-negative bacterial strains, with very high activity against the multidrug-resistant (MDR) *Klebsiella pneumoniae*.[16,17] This may be related to the pyridyl rings' ability to penetrate the membrane walls of bacteria and the low toxicity of the ruthenium center. Closely related to these bipyridines is 4, 5- diazafluorene-9-one (dafo), a derivative of 1,10-phenanthroline. Its coordination properties are similar to the bipyridines and it also contains a reactive exocyclic ketonic group. Lam *et al.* have reported how some Ru(II) bis(2, 2′-bipyridyl) complexes with N-phenyl-substituted diazafluorenes show a high potency towards methicillin-resistant *Staphylococcus aureus* (MRSA).[18] Several transition metal complexes of dafo Schiff-base ligands have also been reported, which possess interesting applications in catalysis, photochemistry and photo physics, as well as in bioinorganic chemistry.[19] Previous studies in this laboratory have reported a large number of half-sandwich ruthenium, rhodium, and iridium complexes with various N, N bidentate ligands such as azine and pyridyl picolinichydrazine.[20]

One of the structural features of dafo derived ligands is their rigid and planar structure, where the ligands can coordinate to the metal atoms in a steric accessible manner. Based on all the findings gathered above and our interest in the chemistry of dafo and its derivatives, here we report the synthesis and characterization of a series of arene platinum group metal complexes {arene = benzene, *p*-cymene and Cp*} with dafo derived N, N bidentate ligands. The free ligands and their complexes have also been analyzed for their antimicrobial and antioxidant activities. Ligands used in the present study are shown in Chart 1.

2. Experimental

2.1 *Physical methods and materials*

All the reagents required for this work were obtained from commercial sources and used as received. The solvents used for synthesis were dried and distilled before use according to the standard procedures. 1,10-phenanthroline, potassium permanganate, aniline and phenyl hydrazine were acquired from Alfa Aesar. The precursor ruthenium complex $[(arene)RuCl_2]_2$ was synthesized following the reported procedure[21] and $[Cp^*MCl_2]_2$ (M = Rh/Ir) complexes were prepared using a synthesizer, Anton par mono-wave 50.[22] 4,5 diazafluorene-9-one (dafo) was synthesized according to the literature method[23] (Scheme 1). The complexes were characterized by various spectroscopic techniques. NMR spectra were recorded on a Bruker Advance II 400 MHz spectrometer using $CDCl_3$ and DMSO as solvents for ^1H NMR with TMS as a standard reference. Infrared spectra (KBr pellets; 400–4000 cm^{-1}) were recorded on a Perkin Elmer 983 spectrophotometer. Mass spectra for the representative complexes were recorded on a Waters UPLC-TQD Mass spectrometer using chloroform as the solvent. The absorption spectra for the complexes were recorded on a Perkin Elmer Lambda 25 UV-vis spectrophotometer in the range of 200–600 nm using acetonitrile at room temperature.

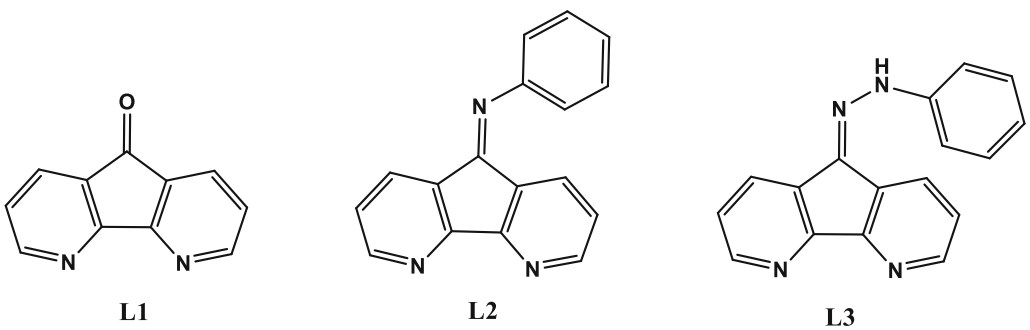

Chart 1. Ligands used in this study.

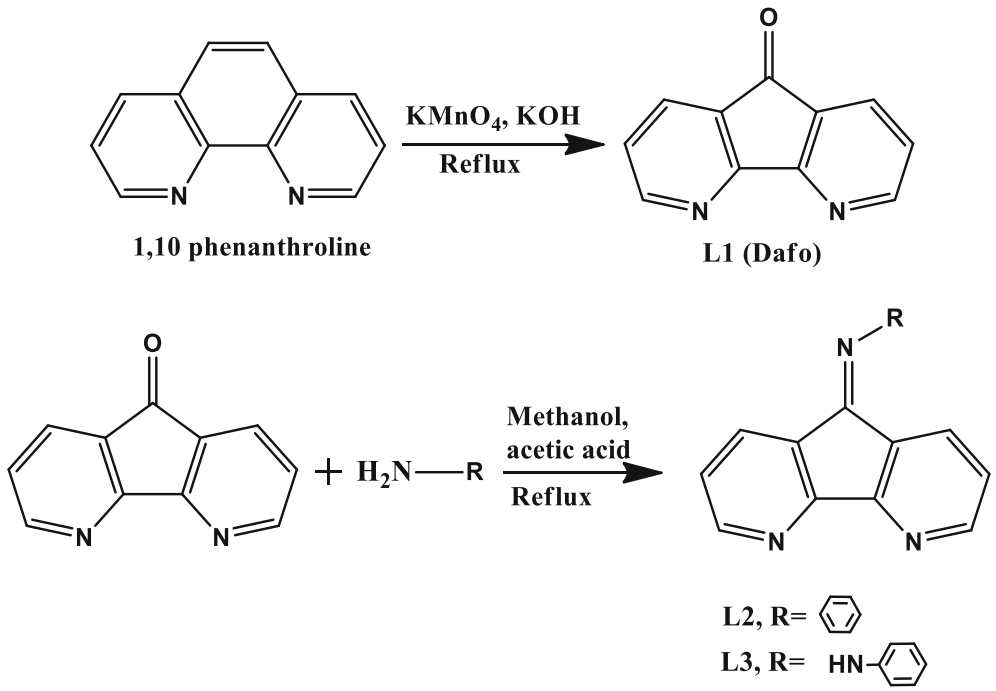

Scheme 1. Preparation of Ligands.

2.2 *Structure determination by X-ray crystallography*

Suitable single crystals of complexes (**1**, **2** and **3**) were grown by slow diffusion of hexane over a dichloromethane solution of the respective complexes. Single crystal X-ray diffraction data for the complexes were collected on an XtaLAB AFC12 (RINC): Kappa single diffractometer using graphite monochromated Mo-Kα radiation (λ=0.7107 Å). Data processing was undertaken with CrysAlisPro CCD software.[24] The structures were solved with the SHELXT structure solution program using Intrinsic Phasing and refined with the SHELXL refinement package using Least Squares minimization.[25,26] The positions of all the atoms were obtained by direct methods. The hydrogen atoms bound to the carbon were placed in geometrically constrained positions and refined with isotropic temperature factors, generally 1.2 U_{eq} of their parent atoms. All non-hydrogen atoms were refined anisotropically. Further details such as crystallographic data and structure refinement details of the complexes are summarized in Table 1 and selected bond lengths and bond angles are listed in Table 2. Figure 1 was drawn by using ORTEP 3 program.[27]

2.3 *In vitro antimicrobial assay*

The antimicrobial activity of the ligands **L1**–**L3** and the newly synthesized complexes was evaluated by the agar well diffusion method. The diameter of the zone of inhibition indicates the degree of sensitivity of the microorganisms to the compound that each well contains. All strains were tested for purity by standard microbiological methods. The test organisms included two Gram-positive (*Staphylococcus aureus* and *Bacillus thuringiensis*) and two Gram-negative (*Escherichia coli* and *Pseudomonas aeruginosa*) bacterial strains. The bacterial stock cultures were maintained on Mueller-Hinton agar slants and stored at 4°C. DMSO was used as a negative control. The bacterial strains were reactivated from stock cultures by transferring into Mueller-Hinton broth and incubating at 37 °C for 24 h. A final inoculum containing 10^6 colonies forming units (1 x 10^6 CFU/mL) was added aseptically to MHA medium and poured into sterile petri dishes. Different test compounds at a concentration of 200 µg per well were added to wells (8 mm in diameter) punched on the agar surface. Plates were incubated overnight at 37 °C and the diameter of the inhibition zone (DIZ) around each well was measured in mm. Experiments were performed in triplicates and these data were presented in Table 3.

Table 1. Crystal structure data and refinement of complexes **1**, **2** and **3**.

Complexes	[**1**]PF_6	[**2**]PF_6	[**3**]PF_6
Empirical formula	$C_{17}H_{12}ClF_6N_2OPRu$	$C_{21}H_{21}ClF_6N_2OPRh$	$C_{21}H_{21}ClF_6IrN_2OP$
Formula weight	541.78	600.73	690.02
Temperature (K)	99.99(10)	302.18(10)	239.99(10)
Wavelength (Å)	0.71073	0.71073	0.71073
Crystal system	monoclinic	triclinic	triclinic
Space group	$P2_1/c$	P_1	P_1
a (Å)/α (°)	8.0024(3)/ 90	8.1020(2)/78.156(2)	8.0906(2)/78.044(2)
b (Å)/β (°)	8.2356(3)/ 96.194(3)	11.7409(3)/81.143(2)	11.7106(3)/80.703(2)
c (Å)/γ (°)	27.5168(8)/90	13.0290(4)/77.058(2)	12.8994(3)/76.687(2)
Volume ($Å^3$)	1802.90(11)	1174.58(6)	1155.17(5)
Z	4	2	2
Density (calc) (Mg/m^{-3})	1.996	1.699	1.984
Absorption coefficient	1.178	0.973	6.029
F(000)	1064.0	600.0	664.0
Crystal size (mm^3)	0.21 × 0.17 × 0.14	0.25 × 0.24 × 0.22	0.16 × 0.12 × 0.08
Theta range for data collection	5.166 to 57.99	5.192 to 57.842	5.212 to 57.97
Index ranges	$-10 \le h \le 10$, $-9 \le k \le 11$, $-36 \le l \le 35$	$-10 \le h \le 10$, $-12 \le k \le 15$, $-17 \le l \le 17$	$-10 \le h \le 10$, $-15 \le k \le 14$, $-17 \le l \le 16$
Reflections collected	14131	16845	16899
Independent reflections	4134 [R_{int} = 0.0256, R_{sigma} = 0.0257]	5406 [R_{int} = 0.0556, R_{sigma} = 0.0492]	5298 [R_{int} = 0.0625, R_{sigma} = 0.0554]
Completeness to theta = 25.00°	99.57	99.6	99.58
Absorption correction	Semi-empirical from equivalents	Semi-empirical from equivalents	Semi-empirical from equivalents
Refinement method	Full-matrix least-squares on F^2	Full-matrix least-squares on F^2	Full-matrix least-squares on F^2
Data/restraints/parameters	4134/0/256	5406/0/303	5298/0/303
Goodness-of-fit on F_2	1.053	1.084	1.056
Final R indices [I>2sigma(I)]	R_1 = 0.0260, wR_2 = 0.0542	R_1 = 0.0412, wR_2 = 0.1109	R_1 = 0.0308, wR_2 = 0.0676
R indices (all data)	R_1 = 0.0293, wR_2 = 0.0555	R_1 = 0.0489, wR_2 = 0.118	R_1 = 0.0350, wR_2 = 0.0690
Absolute structure parameter	n/a	n/a	n/a
Largest diff. peak and hole ($e.Å^{-3}$)	0.61/-0.41	0.90/-0.68	0.89/-1.78
CCDC No.	2046302	2046303	2046304

Structures were refined on F_0^2: $wR_2 = [\Sigma[w(F_0^2 - F_c^2)^2] / \Sigma w(F_0^2)^2]^{1/2}$, where $w^{-1} = [\Sigma(F_0^2)+(aP)^2+bP]$ and $P = [\max(F_0^2, 0)+2F_c^2]/3$.

Table 2. Selected bond lengths (Å) and bond angles (°) of complexes.

Complexes	**1**	**2**	**3**
M(1)-CNT	1.667	1.769	1.770
M(1)-Cl(1)	2.3903(5)	2.3910(10)	2.3958(11)
M(1)-N(1)	2.1334(17)	2.197(3)	2.148(3)
M(1)-N(2)	2.1440(18)	2.178(3)	2.172(3)
N(1)-M(1)-N(2)	80.34(7)	80.21(9)	79.42(11)
N(1)-M(1)-Cl(1)	82.15(5)	88.04(8)	83.36(9)
N(2)-M(1)-Cl(1)	82.97(5)	84.81(8)	85.89(9)

CNT represents the centroid of the arene/Cp* ring and (M = Ru, Rh and Ir).

2.4 *DPPH free radical scavenging assay*

The DPPH radical scavenging activity of the compounds was measured according to the literature method.[28] This method is based on measuring the scavenging capacity of antioxidants towards DPPH 100 µL of methanolic solutions of various concentrations (20–100 µM) of the experimental standard ascorbic acid and the ligands and different concentrations (2–10 µM) of the complexes were taken. About 4 mL of a 0.1 mM methanolic solution of DPPH was added to the 100 µL of the methanolic solution of the samples and standard (vitamin C) and shaken vigorously. Negative control was prepared by adding 100 µL of methanol in 4 mL of 0.1 mM methanolic DPPH solution. The tubes were allowed to stand for 20 min at 27 °C. The absorbance of the sample was measured at 517 nm against the blank (methanol) using a UV-vis spectrophotometer. The potency of scavenging the DPPH radical was calculated by measuring the percentage inhibition, i.e., % DRSA = $\{(A_0 - A_1)/A_0) \times 100\}$ where A_0 is the absorbance of the control reaction, and A_1 is the absorbance of the sample considered.

2.5 *General procedure for the synthesis of metal complexes (1-11)*

To a solution of metal precursor $[(arene)RuCl_2]_2$ (arene = p-cymene, benzene) and $[Cp^*MCl_2]_2$ (M = Rh/Ir) complexes (0.1 mmol), dafo and derived ligands (**L1**, **L2** and **L3**) (0.2 mmol) were added and stirred at room temperature in dry methanol (10 mL) for 1 hour. The counter ion NH_4PF_6 was then added, where the product precipitated out immediately from the reaction mixture. Stirring was continued for another 2 h for completion of the reaction. The precipitate was centrifuged, washed with cold methanol (2–5 mL) and diethyl ether (2–10 mL) and air-dried (Scheme 2).

2.5a *[(benzene)Ru(L1)Cl]PF_6 (1)*: Yield: 92%; Color: Yellow; IR (KBr, cm^{-1}): 1716 $\nu_{(C=O)}$, 1598 $\nu_{(C=N)}$, 1562 $\nu_{(C=C)}$, 843 $\nu_{(P-F)}$. ^{1}H NMR (400 MHz, Chloroform-*d*): δ 8.81 (d, J = 4 Hz, 2H), 8.0 (d, J = 8 Hz, 2H), 7.35 (t, J = 8 Hz, 2H), 7.26 (s, 6H); ^{13}C NMR

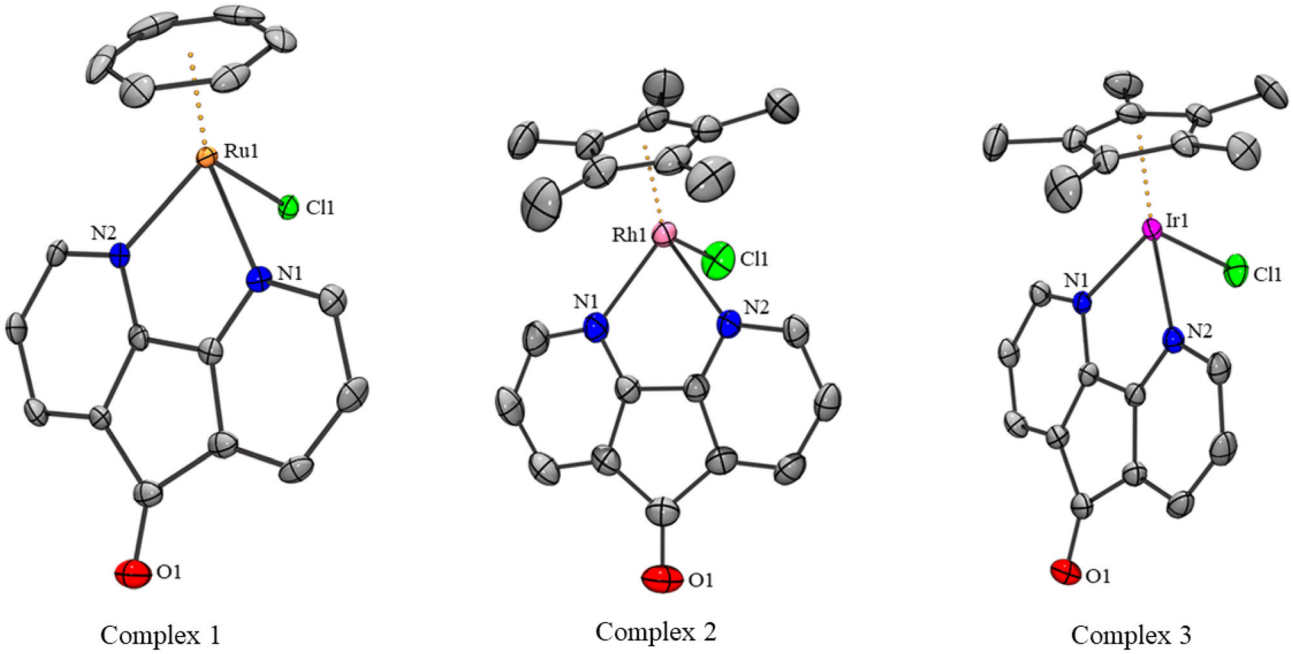

Complex 1 Complex 2 Complex 3

Figure 1. ORTEP diagram of complexes **1**, **2** and **3** with 50% probability thermal ellipsoids. Hydrogen atoms and counter ions are omitted for clarity.

Table 3. Antibacterial activity (Agar well) of tested compounds at concentration 5 mg/mL against different bacterial strains.

		Bacterial Strains			
		Gram –ve		Gram +ve	
Sl. No.	Compounds	*E. coli*	*P. aeruginosa*	*S. aureus*	*B. thuringiensis*
	Kanamycin (+ve control)	21±1	20±1	21±1	20±1
1	Ligand 1	–	–	–	–
2	Complex 1	–	–	–	–
3	Complex 2	–	–	–	–
4	Complex 3	–	–	–	–
5	Ligand 2	–	–	–	–
6	Complex 4	–	–	–	–
7	Complex 5	–	–	–	–
8	Complex 6	–	–	–	–
9	Complex 7	–	–	–	–
10	Ligand 3	–	–	–	–
11	Complex 8	–	–	**20±1**	**20±1**
12	Complex 9	–	–	18±1	18±1
13	Complex 10	–	–	–	–
14	Complex 11	–	–	18±1	18±1

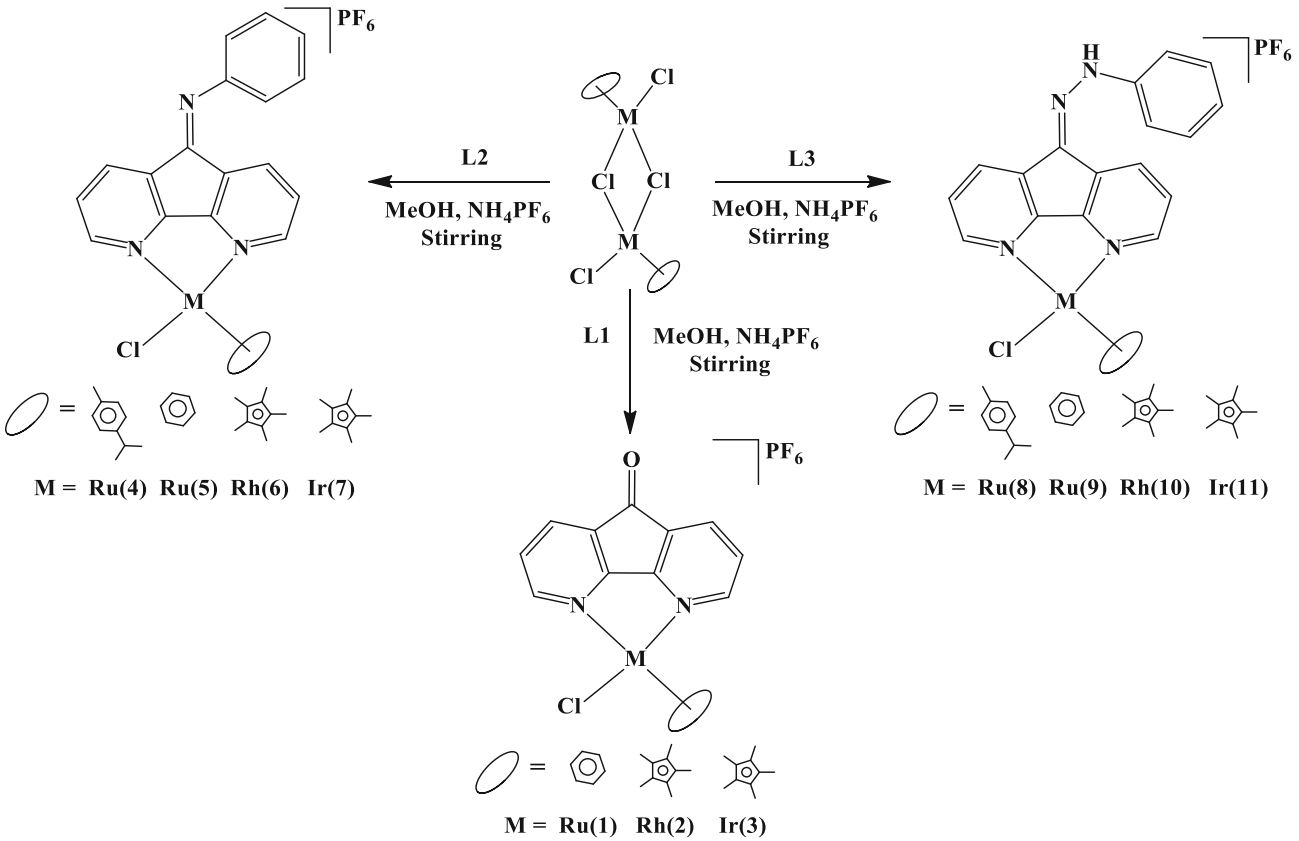

Scheme 2. Schematic representation for the syntheses of complexes.

(100 MHz, DMSO-d_6, ppm): δ 164.57, 162.78, 156.74, 154.89, 135.01, 131.60, 129.20, 125.24, 94.92, 87.63, 84.36; UV-vis {Acetonitrile, λ_{max} nm (ε, 10^4 M^{-1} cm^{-1})}: 235 (4.330), 318 (2.625), 413 (1.201); ESI-MS (*m/z*): 396.9 $[M\text{-}PF_6]^+$, 398.9 $[M\text{-}PF_6+2H]^+$.

2.5b *[Cp*Rh(L1)Cl]PF_6 (2)*: Yield: 90%; Color: Orange; IR (KBr, cm^{-1}): 1716 $\nu_{(C=O)}$, 1598 $\nu_{(C=N)}$, 1562 $\nu_{(C=C)}$, 843 $\nu_{(P\text{-}F)}$. ^{1}H NMR (400 MHz, Chloroform-*d*): δ 8.9 (d, *J* = 4 Hz, 2H), 8.3 (d, *J* = 4 Hz, 2H), 7.9 (t, *J* = 8 Hz, 2H), 1.84 (s, 15H); ^{13}C NMR (100 MHz, $CDCl_3$+ DMSO-d_6, ppm): δ 183.69, 157.46, 149.38, 147.68, 129.52, 126.08, 123.66, 119.52, 93.61, 90.82, 3.36; UV-vis {Acetonitrile, λ_{max} nm (ε, 10^4 M^{-1} cm^{-1})}: 236 (6.200), 302 (2.115), 370 (1.512).

2.5c *[Cp*Ir(L1)Cl]PF_6 (3)*: Yield: 90%; Color: Yellow; IR (KBr, cm^{-1}): 1716 $\nu_{(C=O)}$, 1598 $\nu_{(C=N)}$, 1562 $\nu_{(C=C)}$, 843 $\nu_{(P\text{-}F)}$.^{1}H NMR (400 MHz, Chloroform-*d*): δ 9.0 (d, *J* = 4 Hz, 1H), 8.78 (d, *J* = 8 Hz, 1H), 8.42 (d, *J* = 8Hz, 1H), 8.06 (d, *J* = 8 Hz, 1H), 7.9 (t, *J* = 8 Hz, 1H), 7.47 (t, *J* = 8 Hz, 1H) 1.78 (s, 15H); ^{13}C NMR (100 MHz, $CDCl_3$+ DMSO-d_6, ppm): δ 206.19, 162.67, 154.58, 131.27, 128.90, 124.80, 92.03, 8.09; UV-vis {Acetonitrile, λ_{max} nm (ε, 10^4 M^{-1} cm^{-1})}: 243 (5.525), 317 (2.333), 375 (1.404).

2.5d *[(p-cymene)Ru(L2)Cl]PF_6 (4)*: Yield: 88%; Color: Orange; IR (KBr, cm^{-1}): 1609-1543 $\nu_{(C=N)}$, 1562 $\nu_{(C=C)}$, 843 $\nu_{(P\text{-}F)}$. ^{1}H NMR (400 MHz, Chloroform-*d*): δ 9.36 (d, *J* = 4 Hz, 1H), 9.23 (d, *J* = 8 Hz, 1H), 8.48 (d, *J* = 8 Hz, 1H), 7.86 (d, *J* = 4 Hz, 1H), 7.35 (t, *J* = 8 Hz, 2H), 7.49 (d, *J* = 8 Hz, 2H), 7.04 (t, *J* = 8 Hz, 3H), 6.0 (d, *J* = 4 Hz, 2H), 6.17 (t, *J* = 8 Hz, 2H), 2.83 (sept, *J* = 8 Hz, 1H), 2.26 (s, 3H), 1.20 (d, *J* = 8 Hz, 6H); ^{13}C NMR (100 MHz, $CDCl_3$+ DMSO-d_6, ppm): δ 154.52, 148.66, 136.09, 131.28, 129.20, 128.37, 127.76, 125.33, 118.17, 117.60, 104.41, 100.26, 88.46, 85.31, 82.63, 81.30, 30.62, 29.96, 21.70, 21.39, 18.17, 17.85; UV-vis {Acetonitrile, λ_{max} nm (ε, 10^4 M^{-1} cm^{-1})}: 233 (7.227), 319 (3.067), 415 (1.570).

2.5e *[(benzene)Ru(L2)Cl]PF_6 (5)*: Yield: 88%; Color: Orange; IR (KBr, cm^{-1}): 1609-1543 $\nu_{(C=N)}$, 1562 $\nu_{(C=C)}$, 843 $\nu_{(P\text{-}F)}$. ^{1}H NMR (400 MHz, DMSO-*d*): δ 9.45 (d, *J* = 4 Hz, 1H), 9.33 (d, *J* = 4 Hz, 1H), 8.58 (d, *J* = 4 Hz, 1H), 7.61 (t, *J* = 8 Hz, 1H), 7.53 (t, *J* = 8 Hz, 3H), 7.37 (t, *J* = 8 Hz, 1H), 7.14 (d, *J* = 8 Hz, 2H), 6.97 (d, *J* = 12Hz, 1H), 6.30 (s, 6H); UV-vis {Acetonitrile, λ_{max} nm (ε, 10^4 M^{-1} cm^{-1})}: 233 (5.313), 316 (2.673), 432 (1.499).

2.5f *[Cp*Rh(L2)Cl]PF_6 (6)*: Yield: 85%; Color: Yellow; IR (KBr, cm^{-1}): 1609-1543 $\nu_{(C=N)}$, 1562 $\nu_{(C=C)}$, 843 $\nu_{(P\text{-}F)}$. ^{1}H NMR (400 MHz, Chloroform-*d*): δ 8.92 (d, *J* = 4 Hz, 1H), 8.78 (d, *J* = 8 Hz, 1H), 8.53 (d, *J* = 8 Hz, 1H), 7.92 (t, *J* = 8 Hz, 1H), 7.54 (t, *J* = 8 Hz, 1H), 7.49 (t, *J* = 8 Hz, 2H), 7.36 (t, *J* = 8 Hz, 1H), 7.13 (d, *J* = 8 Hz, 1H), 7.04 (d, *J* = 8 Hz, 2H), 1.85 (s, 15H); ^{13}C NMR (100 MHz, $CDCl_3$+ DMSO-d_6, ppm): δ 161.64, 160.61, 156.66, 151.29, 151.14, 148.91, 136.21, 133.83, 129.25, 128.83, 128.22, 125.94, 118.02, 96.09, 8.84; UV-vis {Acetonitrile, λ_{max} nm (ε, 10^4 M^{-1} cm^{-1})}: 233 (7.589), 314 (2.618), 400 (1.541).

2.5g *[Cp*Ir(L2)Cl]PF_6 (7)*: Yield: 86%; Color: Yellow; IR (KBr, cm^{-1}): 1609-1543 $\nu_{(C=N)}$, 1562 $\nu_{(C=C)}$, 843 $\nu_{(P\text{-}F)}$. ^{1}H NMR (400 MHz, Chloroform-*d*): δ 8.91 (d, *J* = 4 Hz, 1H), 8.78 (d, *J* = 4 Hz, 1H), 8.56 (d, *J* = 8 Hz, 1H), 7.94 (t, *J* = 8 Hz, 1H), 7.57 (t, *J* = 8 Hz, 1H), 7.51 (t, *J* = 8 Hz, 2H), 7.38 (t, *J* = 8 Hz, 1H), 7.17 (d, *J* = 8 Hz, 1H), 7.08 (d, *J* = 8 Hz, 2H), 1.83 (s, 15H); UV-vis {Acetonitrile, λ_{max} nm (ε, 10^4 M^{-1} cm^{-1})}: 234 (6.060), 314 (2.623), 415 (1.430); ESI-MS (*m/z*): 620.1 $[M\text{-}PF_6]^+$, 622.1 $[M\text{-}PF_6+2H]^+$.

2.5h *[(p-cymene)Ru(L3)Cl]PF_6 (8)*: Yield: 88%; Color: Orange; IR (KBr, cm^{-1}): 3400$\nu_{(N\text{-}H)}$, 1609-1543 $\nu_{(C=N)}$, 1562 $\nu_{(C=C)}$, 843 $\nu_{(P\text{-}F)}$. ^{1}H NMR (400 MHz, Chloroform-*d*): δ 11.21 (s, 1H), 9.17 (t, *J* = 8 Hz, 2H), 9.12 (d, *J* = 4 Hz, 1H), 8.40 (d, *J* = 8 Hz, 1H), 7.79 (d, *J* = 8 Hz, 1H), 7.71 (d, *J* = 8 Hz, 1H), 7.60 (d, *J* = 8 Hz, 2H), 7.38 (t, *J* = 8 Hz, 2H), 7.11 (t, *J* = 8 Hz, 1H), 6.12 (d, *J* = 4 Hz, 2H), 5.95 (t, *J* = 8 Hz, 2H), 2.80 (sept, *J* = 8 Hz, 1H), 2.28 (s, 3H), 1.15 (t, *J* = 4 Hz, 6H); UV-vis {Acetonitrile, λ_{max} nm (ε, 10^4 M^{-1} cm^{-1})}: 239 (4.532), 300 (2.859), 415 (4.913); ESI-MS (*m/z*): 543.0 $[M\text{-}PF_6]^+$, 545.0 $[M\text{-}PF_6+2H]^+$.

2.5i *[(benzene)Ru(L3)Cl]PF_6 (9)*: Yield: 86%; Color: Yellow; IR (KBr, cm^{-1}): 3400 $\nu_{(N\text{-}H)}$, 1609-1543 $\nu_{(C=N)}$, 1562 $\nu_{(C=C)}$, 843 $\nu_{(P\text{-}F)}$. ^{1}H NMR (400 MHz, DMSO-*d*): δ 9.33 (s, 1H), 9.12 (d, *J* = 8 Hz, 1H), 8.50 (d, *J* = 8 Hz, 1H), 7.92 (d, 1H), 7.81 (t, 1H), 7.62 (d, *J* = 8 Hz, 3H), 7.41 (t, *J* = 8 Hz, 3H), 7.10 (t, *J* = 8 Hz, 1H), 6.29 (s, 6H); UV-vis {Acetonitrile, λ_{max} nm (ε, 10^4 M^{-1} cm^{-1})}: 236 (4.300), 298 (2.890), 414 (4.349).

2.5j *[Cp*Rh(L3)Cl]PF_6 (10)*: Yield: 92%; Color: Yellow; IR (KBr, cm^{-1}): 3400 $\nu_{(N\text{-}H)}$, 1609-1543 $\nu_{(C=N)}$, 1562$\nu_{(C=C)}$, 843 $\nu_{(P\text{-}F)}$.^{1}H NMR (400 MHz, Chloroform-*d*): δ 11.13 (s, 1H), 9.18 (d, *J* = 8 Hz, 1H),

8.72 (d, J = 4 Hz, 1H), 8.66 (d, J = 8 Hz, 1H), 8.44 (d, J = 8 Hz, 1H), 7.83 (t, J = 8 Hz, 1H), 7.77 (t, J = 8 Hz, 1H), 7.60 (d, J = 8 Hz, 2H), 7.40 (t, J = 8 Hz, 3H), 1.85 (s, 15H); UV-vis {Acetonitrile, λ_{max} nm (ε, 10^4 M^{-1} cm^{-1})}: 233 (7.462), 297 (3.088), 412 (5.668); ESI-MS (*m/z*): 545.1 $[M\text{-}PF_6]^+$, 547.0 $[M\text{-}PF_6{+}2H]^+$.

2.5k *[Cp*Ir(L3)Cl]PF_6 (11)*: Yield: 90%; Color: Yellow; IR (KBr, cm^{-1}): 3400 $\nu_{(N\text{-}H)}$, 1609-1543 $\nu_{(C=N)}$, 1562$\nu_{(C=C)}$, 843 $\nu_{(P\text{-}F)}$.^{1}H NMR (400 MHz, Chloroform-*d*): δ 11.13 (s, 1H), 9.16 (d, J = 8 Hz, 1H), 8.65 (d, J = 4 Hz, 1H), 8.58 (d, J = 4 Hz, 1H), 8.42 (d, J = 8 Hz, 1H), 7.82 (t, J = 8 Hz, 1H), 7.74 (t, J = 8 Hz, 1H), 7.61 (d, J = 8 Hz, 2H), 7.41 (t, J = 8 Hz, 2H), 7.14 (t, J = 8 Hz, 1H), 1.84 (s, 15H); UV-vis {Acetonitrile, λ_{max} nm (ε, 10^4 M^{-1} cm^{-1})}: 231 (4.570), 297 (3.280), 414 (5.184).

3. Results and Discussions

3.1 *Synthesis of metal complexes*

All the metal complexes were synthesized[29] by the reaction of the respective metal precursors with dafo and derived ligands **L1-L3** in dry methanol for 3 h in the ratio of 1:2 (M:L). The ligands bind to the metal centers *via* the N, N donor atoms as confirmed by X-ray crystallography. The complexes were isolated as analytically pure hexafluorophosphate salts, which are represented in Scheme 2. These salts are non-hygroscopic and stable in the air as well as in a solution. They are soluble in common organic polar solvents but are insoluble in non-polar solvents. All the compounds are characterized by ^{1}H NMR, ^{13}C NMR, UV-vis, IR spectroscopy and Mass spectrometry.

3.2 *Spectral studies of the complexes*

3.2a *FT-IR studies*: IR spectrum of ligand **L1** contains a peak at 1719 cm^{-1} which corresponds to the C=O vibration band of the carbonyl group. The formation of the C=N bond in ligands **L2** and **L3** can be proved by the disappearance of the peak at 1719 cm^{-1} and the appearance of a new peak around 1637–1656 cm^{-1} which corresponds to the vibration band of the resultant azomethine, C=N group. This indicates the occurrence of the condensation reaction and the subsequent formation of the ligands. The presence of the NH group in ligand **L3** is confirmed by the stretching frequency at around 3424 cm^{-1}. Besides, the IR spectra of the free ligands also exhibit the characteristic bands due to C=N (pyridine) and C=C (aromatic) at 1591–1600 cm^{-1} and 1558–1567 $cm^{-1,}$ respectively. Upon coordination of the ligands with the metal dimers, the IR spectra of the complexes undergo a slight change whereby the bands due to C=N (pyridine) shifted to a lower wavenumber indicating the coordination of the metals to the ligands through the pyridine nitrogen atoms. Furthermore, the presence of the PF_6 counter ion in all the complexes is evident from the IR absorption band between 835 and 847 cm^{-1}.

3.2b *NMR spectral studies*: The ^{1}H NMR spectra of complexes **1–11** display signals featuring the ligands, arene and cyclopentadienyl rings. A characteristic pattern comprising doublets and triplets is observed in all complexes associated with the protons of the unsubstituted ring of 4, 5 diazafluorene moiety. The doublets are observed between 7.13–9.18 ppm and the triplets are observed in the range of 7.35–9.17 ppm. The aromatic proton signals associated with the ligands **L2** and **L3** are observed as doublets and triplets in the range of 7.35–9.17 ppm. The ^{1}H NMR spectra of complexes **8–11** show a singlet in the range of 9.33–11.21 ppm due to NH proton. The appearance of this N-H signal is in good agreement with the appearance of NH stretching frequency as revealed from FT-IR spectroscopy. In all the complexes, the protons that are adjacent to the nitrogen atoms of 4, 5 diazafluorene moiety exhibit doublets which are downfield than the other peaks indicating coordination of the ligands to the metal ions. The benzene proton resonance in complexes **1, 5** and **9** is observed as a singlet around 6.29–7.26 ppm. For complex **1,** the benzene proton resonance is observed at 7.26 ppm, which coincides with the solvent signal of $CDCl_3$. In the *p*-cymene ruthenium complexes, an unusual splitting pattern was observed for the aromatic protons as well as the isopropyl protons. Instead of two doublets, the aromatic protons of the p-cymene moiety split into one doublet and one triplet around 5.95–6.17 ppm. Also, the isopropyl group split into one doublet for **4** and one triplet for **8** around 1.15–1.20 ppm. The splitting of the aromatic and isopropyl groups of the *p*-cymene moiety is due to the loss of symmetry of the *p*-cymene group upon coordination with the ligands. This unusual pattern of the splitting of *p*-cymene is relatable to the metal center being diastereotopic and chiral upon coordination of the ligand and correlates well with related complexes.[30] The spectra of the complexes also exhibited one septet around 2.80–2.83 ppm for the methine protons of the isopropyl group and a singlet

around 2.26–2.28 ppm for the methyl protons. In addition to these proton signals, a sharp singlet is observed around 1.78–1.85 ppm for the methyl protons of the Cp* ligand for the rhodium and iridium complexes.

3.2c *^{13}C NMR spectra of complexes*: ^{13}C NMR spectroscopy gives valuable structural information about the presence of different carbon atoms present in a compound. The ^{13}C NMR spectra of the representative complexes are provided in the supplementary data (Figures S12-16, SI). The results obtained strongly support the formation of metal complexes. The ^{13}C NMR spectra of the complexes exhibited signals associated with the ligand carbons, benzene ring carbons, *p*-cymene ligand carbons, ring carbons of Cp* and methyl carbons of Cp*. The carbon resonances of the carbonyl (C=O) group appeared in the lower frequency region in the range of 164.57–206.19 ppm. The carbon resonances of the imine (C=N) group were observed around 154.52–162.67 ppm. The aromatic carbon resonances for the ligands were observed in the range of 117.60–162.78 ppm. The ring carbon resonances of the benzene ligand were observed around 84.36–94.92 ppm. The ring carbon resonances of the *p*-cymene ligand were observed around 81.30–104.41 ppm. The methyl, methine and isopropyl carbon resonances of *p*-cymene ligand were observed in the range between 17.85–39.71 ppm. The signals associated with the ring carbons of the Cp* ligand were observed in the region around 92.03–96.09 ppm. The methyl carbon resonances of the Cp* ligand were observed as a sharp peak around 3.36–8.84 ppm.

3.2d *Mass spectra of complexes*: The mass spectrum can be used as a "chemical fingerprint" as it is unique for each compound. The electron impact mass spectra of the complexes are recorded and analyzed at an electron energy of 70 eV. The molecular ion peaks are in good agreement with the suggested empirical formula. The mass spectra of complexes **1**, **7**, **8** and **10** are given in supplementary data (Figures S17-20). All the complexes show prominent molecular ion peaks corresponding to $[M\text{-}PF_6]^+$ and $[M\text{-}PF_6+2H]^+$ ions. In the mass spectra of the complexes (**1**, **7**, **8** and **10**), the peaks at m/z: 396.9, m/z: 620.1, m/z: 543.0 and m/z: 545.1 can be assigned as $[M\text{-}PF_6]^+$ ion peaks, respectively. Whereas the peaks at m/z: 398.9, m/z: 622.1, m/z: 545.0 and m/z: 547.0 can be assigned as $[M\text{-}PF_6+2H]^+$ ion peaks, respectively.

3.2e *UV-Visible studies of the complexes*: The electronic spectra of all the complexes **1–11** were recorded in acetonitrile at 10^{-4}M concentration at room temperature and the plot is shown in Figure 3. Two distinct sets of absorption bands are present for all complex solutions. The absorption spectra of the complexes exhibit ligand-centered (LC) and metal-to-ligand charge transfer (MLCT) bands. The intense bands found in the UV region of 231–319 nm are assigned to intra-ligand or ligand-centered transitions (π-π* and n-π*) due to transitions involving molecular orbitals located on 4, 5 diazafluorene and the carbonyl group chromophore (for complexes **1–3**) or C=N chromophore. The spectra of the complexes show charge-transfer transitions which can be seen in the range 370–415 nm. Transitions of this type are expected when the metal ion has filled orbitals lying higher than the highest filled ligand orbitals and the ligands possess vacant low-lying orbitals. This significant π back-bonding is particularly interesting for complexes whose ligands (containing CO, pyridine) have empty π antibonding orbitals. The possible MLCT transitions in which both the metal t_{2g} and e^*_g orbitals are occupied and ligand π* orbitals are vacant are $e^*_g \rightarrow \pi^*$ and $t_{2g} \rightarrow \pi^*$. It may also be noted that in complexes **8–11**, the charge transfer (CT) bands are more intense (Hyperchromic shift) compared to the other complexes. This may be due to the extension of conjugation provided by the additional nitrogen atom. The spectra of the complexes, which were recorded immediately and at different time intervals up to 48 hrs, did not show any significant alteration in the intensity of the bands, indicating the stability of the complexes in these solutions at room temperature (Figures S21-23, SI).

3.3 *Single-crystal X-ray structure determination of complexes*

Single crystals suitable for X-ray diffraction analysis were obtained for complexes **1**, **2** and **3**. They were grown by slow diffusion of hexane into dichloromethane solution of the complexes. The summary of the single-crystal X-ray structure analyses is shown in Table 1. Selected bond lengths and bond angles are given in Table 2. The ORTEP drawings, including the atom labeling scheme of complexes **1, 2** and **3** are shown in Figure 1.

Complexes **2** and **3** are isostructural and crystallize in triclinic systems with space group P_1, while complex **1** crystallizes in a monoclinic system with space group *P2/c*. In all the complexes, the metal center is

coordinated to η^6-benzene or η^5-Cp* ligands, two nitrogen donor atoms from chelating ligand in a bidentate $k^2_{(NN')}$ fashion and one terminal chloride leading to the characteristic three-legged "piano stool" structures. The geometry around the metal center can be regarded as distorted octahedral if the η^6-benzene or η^5-Cp* moieties are assumed to occupy three facial-coordinated positions acting as a seat of the piano stool and the nitrogen donor atoms from dafo ligand and terminal chloride are legs. The ligand coordinated to the metal center in a neutral bidentate chelating manner through the pyridine nitrogen atoms forming a five-membered metallocycle. The deviation of the coordination sphere from the ideal octahedral geometry is because of the slight bite angle of the five-membered chelate ring. The five-membered chelate rings have an N(1)–M(1)–N(2) bite angle of 80.34(7) for complex **1**, 80.21(9) for complex **2** and 79.42(11) for complex **3**. The distance between the ruthenium atom and the center of the benzene ring is 1.667 Å in complex **1**, whereas the distances of metal to the center of the Cp* ring in rhodium and iridium complexes in complexes **2** and **3** are longer (1.769 Å and 1.770 Å) respectively. These bond lengths are comparable to those in related complexes. The M-N and M–Cl bond lengths in these complexes are comparable to each other and not much variation is observed. The selected bond distances of complexes **1–3** such as M(1)-Cl(1), M(1)-N(1) and M(1)-N(2) and bond angles agree very well with the similarly reported ruthenium(II), rhodium(III) and iridium(III) complexes containing nitrogen donor ligands.[31-35]

3.4 *In vitro antimicrobial activity*

All the synthesized compounds were tested for *in vitro* antibacterial activities against two Gram-positive (*Staphylococcus aureus* and *Bacillus thuringiensis*) and two Gram-negative (*Escherichia coli* and *Pseudomonas aeruginosa*) bacterial strains by the agar well diffusion method using kanamycin as a reference standard. The antibacterial activity of the tested compounds, in terms of the formation of an inhibitory zone at a concentration of 5 mg/mL, is presented in Table 3. It is found that some compounds contribute antibacterial activity against Gram-positive bacterial strains. However, no zone of inhibition was observed against Gram-negative bacterial strains in the ligands or complexes. The results revealed that the dafo and derived Schiff base ligands **L1–L3** show no activity against all the tested bacterial strains. Complexes of **L1** and **L2**, namely, complexes **1–7**, exhibit no activity against any bacterial strain. However, complexes of **L3**, namely, complexes **8**, **9** and **11,** exhibit potent inhibitory activities against *S. aureus* and *B. thuringiensis* with inhibition zone diameters ranging from 18 ± 1 to 20 ± 1 mm. Complex **8** shows the highest activity against the Gram-positive bacterial strains *S. aureus* and *B. thuringiensis* with an inhibition value of 20 ± 1 mm, respectively, which is equivalent to the activity of the positive control kanamycin. Complexes **9** and **11** also show good activity with an inhibition value of 18 ± 1 mm against both *S. aureus* and *B. thuringiensis.* It is noteworthy that the activity of the p-cymene ruthenium complex **8** is more effective compared to its benzene ruthenium and Cp* Iridium counterparts **9** and **11**. Earlier reports have also demonstrated how some p-cymene ruthenium complexes exhibit high potency towards *S. aureus*.[10] Chelation usually increases the toxicity of metal complexes. This can be explained by Tweedy's chelation theory.[36] Coordination reduces the polarity of the metal ion essentially because of the partial sharing of its positive charge with the donor groups within the chelate ring system formed during coordination and leads to an increase in the lipophilic nature of the central metal atom, which favors its permeation more effectively through the lipid layer of the microorganism, thus destroying them more aggressively.[36,37] The MIC values of the compounds are observed in the range of 1.25–2.5 mg/mL against the Gram-positive bacterial strains *S. aureus* and *B. thuringiensis*.

These results show that some synthesized compounds have potent inhibitory activities against Gram-positive bacteria, indicating selective antibacterial agents. Hence, they have an effective antimicrobial potential against the indicated pathogens. Among all the compounds analyzed, complex **8** is found to be the most potent antimicrobial agent against Gram-positive bacteria.

3.5 *Antioxidative activity*

Antioxidants can react with excess free radicals by interfering with the oxidation process and also by acting as reactive species scavenger. DPPH (2,2-diphenyl-1-picryl-hydrazyl) free radical scavenging method is widely used to determine the antioxidant activity. The DPPH antioxidant assay is based on the ability of 2,2-diphenyl-1-picryl-hydrazyl, a stable free radical, to decolorize in the presence of antioxidants. When DPPH accepts an electron donated by an antioxidant, the DPPH is decolorized, which can be

quantitatively measured from the changes in absorbance. The percentage radical scavenging ability of the free ligands and their complexes was tested based on the radical scavenging effect on the DPPH free radical using ascorbic acid as a standard and the results are shown in Figure 2 and Table 4. The results show that the compounds display appreciable radical scavenging activity. Among the tested compounds, at a concentration of 1 mg/mL, the DPPH radical scavenging activity (DRSA %) of complexes **1**, **2**, **3**, **4**, **5**, **6**, **7**, **8**, **9**, **10**, **11** and ligands **L1** and **L3** are around 6.3%, 3.7%, 11%, 7.6%, 8%, 62.5%, 40.6%, 77%, 77%, 81.2%, 80.3%, 1.6% and 95.2%, respectively. **L2** was found to be inactive. The complexes of **L1** and **L2**, namely, **1-7,** show low to moderate radical scavenging activities (Figure 3).

On the other hand, all the complexes containing ligand **L3** show higher antioxidant activity than the other complexes. Also, **L3** showed the highest DPPH scavenging activity (DRSA %), which was almost as potent as ascorbic acid. The antioxidant property of a compound depends on its ability to act as an electron donor or hydrogen donor to a free radical to make it stable. Therefore, the high scavenging activity of **L3** may be due to the presence of the N-H group in the structure of **L3,** which can act as a significant hydrogen donor or reducing agent by neutralizing the free radicals.[38]

This assumption is in agreement with the results obtained from the control experiment. The control experiment can be used as a test to assess the validity of the assumption and the experimental results, often through a comparison of the results between the control and the compounds under study. The control used was a simple Schiff base obtained from benzaldehyde and phenylhydrazine. The radical scavenging ability of the control and the experimental group (**L2**, **L3**) was compared and the results are shown in Figure S26 and Table S1 (SI). The results show that **L3** and the control, containing the NH moiety, exhibit almost identical radical scavenging activity at 96.25% and 96.58%, respectively. In contrast, **L2**, containing no NH moiety, was found to be inactive. This finding indicates that the presence of NH moiety has a significant effect on increasing the antioxidant activity of **L3**. This structural difference influences the radical scavenging activity of the compounds. The conclusion drawn from this study is, therefore, valid.

Table 4. DPPH radical scavenging activity of tested compounds.

Sl. No.	Compound	% DRSA	Std. error
1	AA	100	–
2	Ligand 1	1.6	± 0.8
3	Complex 1	6.3	± 1.4
4	Complex 2	3.7	± 1.1
5	Complex 3	11.0	± 1.9
6	Complex 4	7.6	± 0.7
7	Complex 5	8.0	± 0.2
8	Complex 6	62.5	± 2.8
9	Complex 7	40.6	± 0.9
10	Ligand 3	**95.2**	± 1.4
11	Complex 8	77.0	± 0.1
12	Complex 9	77.0	± 0.9
13	Complex 10	**81.2**	± 0.3
14	Complex 11	**80.3**	± 0.4

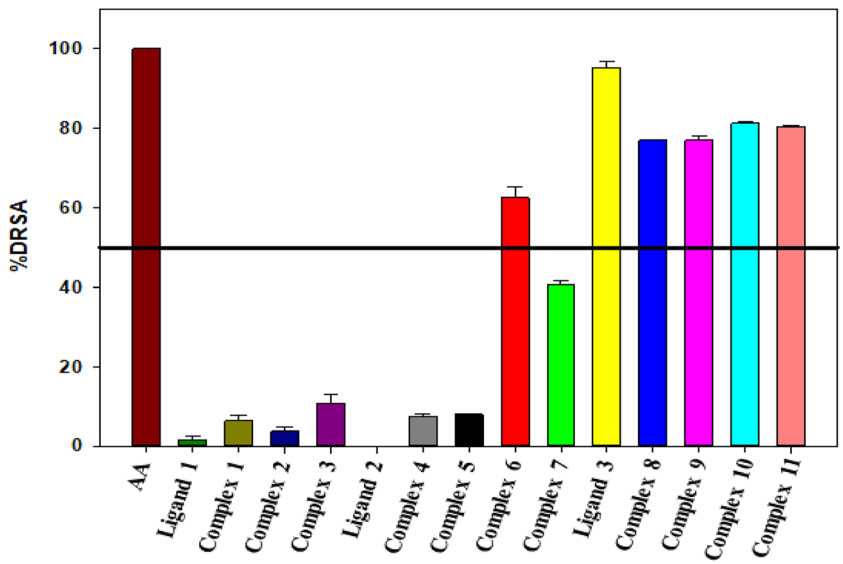

Figure 2. Histogram of the DPPH radical scavenging activity of ligands and complexes compared to ascorbic acid.

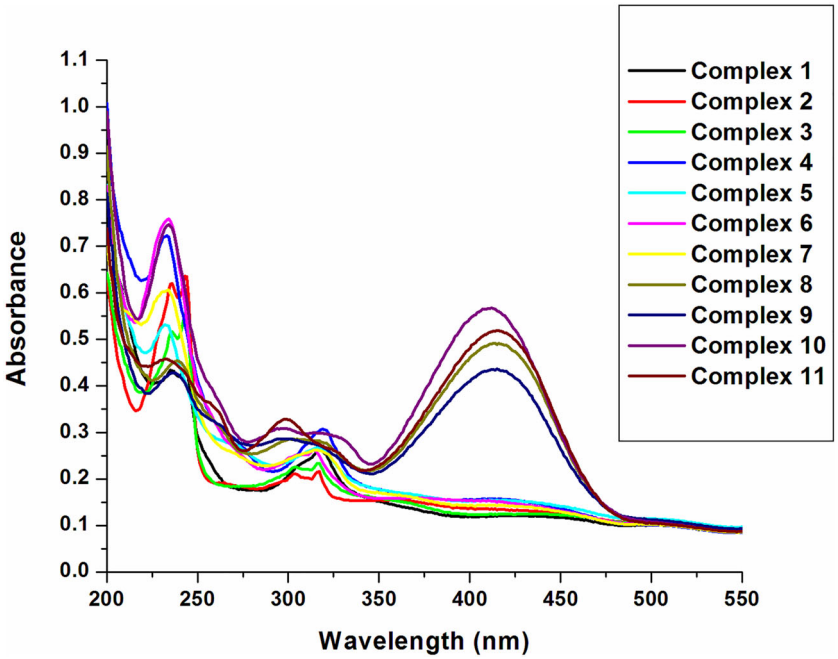

Figure 3. UV-Visible electronic spectra of complexes in acetonitrile at 298 K.

Hence **L3** can act as a powerful antioxidant by scavenging free radicals. However, an exact explanation as to why ligand **L3** shows better scavenging activity than its complexes could not be attained.

3.6 *Structure-activity relationship (SAR)*

The correlation between the structure of the diazafluorene derivative ligands and complexes and their activities can be verified from the results of antimicrobial and antioxidant activities given in Tables 3 and 4 and Figure 3. Even though no exact structure-activity relationship could be determined, some conclusions regarding the the influence of structural changes on the antibacterial and antioxidant activities of the compounds can be obtained by comparing their structures with their activities.

By comparison of the results obtained, the antibacterial activity of the complexes can be related to features such as the presence of an NH moiety and the absence of a carbonyl group. Complexes **8**, **10** and **11** containing **L3** were active against Gram-positive bacterial strains (*S. aureus* and *B. thuringiensis*), while all the other complexes were found to be inactive. These results show that the presence of the NH moiety appears to be an essential requirement for antibacterial activity and selectivity. Also, the radical scavenging activity of a compound is dependent on the molecular structure. The results obtained from antioxidant activities showed that, between complexes of **L1**, **L2** and **L3**, the complexes containing **L3** exhibit better results. Also, **L3** showed the highest DPPH scavenging activity (DRSA %), which was almost as potent as the standard used. This may be attributed to the presence of the N-H group attached to the structure of **L3** and the absence of a carbonyl group, which remarkably increases the activity.

These results indicate that these structural characteristics contribute to a high antibacterial and radical scavenging activity. Based on these results, it seems possible to establish a coherent relationship between the antibacterial and antioxidative activity evaluated for the compounds and the molecular structure of the compounds. Consequently, we can thereby confirm the proposed structure-activity relationship.

4. Conclusions

The NN′ donor, dafo and derived Schiff base ligands, **L1–L3** and their corresponding metal complexes having general formula, [(arene/Cp*)M(L)Cl]PF_6 have been synthesized and characterized by different spectroscopic techniques. The structures of complexes **1–3** have been determined by X-ray crystallography and the ligands were found to coordinate in a neutral bidentate NN′ donor manner. Preliminary biological studies like antibacterial and antioxidant activities were carried out. The antimicrobial studies revealed

that the compounds selectively inhibit only Gram-positive bacterial strains (*S. aureus* and *B. thuringiensis*), thereby acting as selective antibacterial agents. Besides, the results obtained from the DPPH antioxidant assay showed their significant efficacy in scavenging free radicals, with ligand **L3** showing the highest antioxidant activity owing to the presence of the N-H group attached to its structure. It was also interesting to note that the complexes containing ligand **L3** showed high antibacterial and antioxidant activity compared to complexes containing ligands **L1** and **L2**. However, more investigations are needed before we characterize them as biological antibacterials and antioxidants, thereby facilitating research in the pharmaceutical industry.

Supplementary Information (SI)

CCDC: **2046302** (1); **2046303** (2); **2046304** (3) contains the supplementary crystallographic data for this paper. These data can be obtained free of charge via www.ccdc.cam.ac.uk/data_request/cif, by e-mailing data_request@ccdc.cam.ac.uk, or by contacting The Cambridge Crystallographic Data Centre, 12, Union Road, Cambridge CB2 1EZ, UK; Fax: +44 1223 336033. Figures S1-S26 and Table S1 are available at www.ias.ac.in/chemsci.

Acknowledgment

Carley Giffert L Nongpiur is grateful to Larica Pathaw for her help in the initial stages of this work. Carley also thanks Professor A. K. Singh, Department of Biochemistry, NEHU, SAIF-CDRI, Lucknow and SAIF-NEHU, Shillong for spectral analyses.

References

1. Krishnamoorthy M, Hakobyan S, Ramstedt M and Gautrot J E 2014 Surface-initiated polymer brushes in the biomedical field: Applications in membrane science, biosensing, cell culture, regenerative medicine and antibacterial coatings *Chem. Rev.* **114** 10976
2. Li J, Wang G, Zhu H, Zhang M, Zheng X, Di Z, et al. 2014 Antibacterial activity of large-area monolayer graphene film manipulated by charge transfer *Sci. Rep.* **4** 4359
3. Zhang H, Liu H B and Yue J M 2014 Organic carbonates from natural sources *Chem. Rev.* **114** 883
4. Liu R, Chen X, Chakraborty S, Lemke J J, Hayouka Z, Chow C, et al. 2014 Tuning the biological activity profile of antibacterial polymers via subunit substitution pattern *J. Am. Chem. Soc.* **136** 4410
5. Fasciani C, Silvero M J, Anghel M A, Arguello G A, Becerra M C and Scaiano J C 2014 Aspartame-stabilised gold-silver bimetallic biocompatible nanostructures with plasmonic photothermal properties, antibacterial activity, and long-term stability *J. Am. Chem. Soc.* **136** 17394
6. Dodbele S, Martinez C D and Troutman J M 2014 Species differences in alternative substrate utilization by the antibacterial target undecaprenyl pyrophosphate synthase *Biochem.* **53** 5042
7. Levy S B and Marshall B 2004 Antibacterial resistance worldwide: causes, challenges and responses *Nat. Med.* **10** 122
8. Gold H S and Moellering R C 1996 Antimicrobial-drug resistance *N. Engl. J. Med.* **335** 1445
9. Sun D, Zhang W, Lv M, Yang E, Zhao Q and Wang W 2015 Antibacterial activity of ruthenium(II) polypyridyl complex manipulated by membrane permeability and cell morphology *Bioorg. Med. Chem. Lett.* **25** 2068
10. Gichumbi J M, Omondi B, Lazarus G, Singh M, Shaikh N, Chenia H Y and Friedrich H B 2017 Influence of halogen substitution in the ligand sphere on the antitumor and antibacterial activity of half-sandwich ruthenium(II) complexes $[RuX(\eta^6\text{-arene})(C_5H_4N\text{-}2\text{-}CH{=}N\text{-}Ar)]^+$ *Z. Anorg. Allg. Chem.* **643** 699
11. Diengdoh D F 2017 Evaluation of phytochemicals and antioxidant activity in underutilised wild edible plants of Meghalaya state, India *Int. J. ChemTech. Res.* **10** 674
12. Clarke M J 2002 Ruthenium metallopharmaceuticals *Coord. Chem. Rev.* **232** 69
13. Mladenova R, Ignatova M, Manolova N, Petrova T and Rashkov I 2002 Preparation, characterization and biological activity of Schiff base compounds derived from 8-hyroxyquinoline-2-carboxaldehyde and Jeffamines ED® *Eur. Polym. J.* **38** 989
14. Singh K, Barwa M S and Tyagi P 2006 Synthesis, characterization and biological studies of Co(II), Ni(II), Cu(II) and Zn(II) complexes with bidentate Schiff bases derived by heterocyclic ketone *Eur. J. Med. Chem.* **41** 147
15. Panneerselvam P, Nair R R, Vijayalakshmi G, Subramanian E H and Sridhar S K 2005 Synthesis of Schiff bases of 4-(4-aminophenyl)-morpholine as potential antimicrobial agents *Eur. J. Med. Chem.* **40** 225
16. Abebe A and Hailemariam T 2016 Synthesis and assessment of antibacterial activities of ruthenium (III) mixed ligand complexes containing 1, 10-phenanthroline and guanide *Bioinorg. Chem. Appl.* **2016** 1
17. Gopinath K, Karthika V, Gowri S, Senthilkumar V, Kumaresan S and Arumugam A 2014 Antibacterial activity of ruthenium nanoparticles synthesized using Gloriosa superba L. leaf extract *J. Nanostruct. Chem.* **4** 83
18. Lam P L, Lu G L, Hon K M, Lee K W, Ho C L, Wang X, et al. 2014 Development of ruthenium (II) complexes as topical antibiotics against methicillin resistant Staphylococcus aureus *Dalton Trans.* **43** 3949
19. Annibale V T and Song D T 2016 Coordination chemistry and applications of versatile 4,5-diazafluorene derivatives *Dalton Trans.* **45** 32
20. (a) Adhikari S, Kaminsky W and Kollipara M R 2017 Investigation of the coordination chemistry of multidentate azine Shiff-base ligands towards d^6 half-sandwich metal complexes *J. Organomet. Chem.* **848** 95; (b) Palepu N R, Premkumar J R, Verma A K, Bhattacharjee K, Joshi S R, Forbes S, Mozharivskyj Y

and Kollipara M R 2018 Antibacterial, in vitro antitumor activity and structural studies of rhodium and iridium complexes featuring the two positional isomers of pyridine carbaldehyde picolinic hydrazone ligand *Arab. J. Chem* **11** 5 714
21. Bennett M A, Huang T N, Matheson T W, Smith A K, Ittel S and Nickerson W 1982 (η^6-Hexamethylbenzene) Ruthenium complexes *Inorg. Synth.* **21** 74
22. Dkhar L, Kaminsky W, Poluri K M and Kollipara M R 2019 Versatile coordination modes of benzothiazole hydrazone derivatives towards Ru(II), Rh(III) and Ir(III) complexes and their reactivity studies with azides and activated alkynes *J. Organomet. Chem.* **891** 54
23. Henderson L J, Fronczek J F R and Cherry W R 1984 Selective perturbation of ligand field excited states in polypyridine ruthenium(II) complexes *J. Am. Chem. Soc.* **106** 5876
24. Crysalis P R O, release (2012) Version 1.171.36.20. Agilent Technologies, Yarnton
25. Sheldrick G M 2015 SHELXT-Integrated space-group and crystal-structure determination *Acta Cryst. A* **71** 3
26. Sheldrick G M 2015 Crystal structure refinement with SHELXL *Acta Cryst. C* **71** 3
27. Farrugia L J 1997 ORTEP-3 for Windows-a version of ORTEP-III with a Graphical User Interface (GUI) *J. Appl. Crystallogr.* **30** 565
28. Blois M S 1958 Antioxidant determinations by the use of a stable free radical *Nature* **181** 1199
29. Baran M F, Durap F, Aydemir M and Baysal A 2016 Transfer hydrogenation of aryl ketones with homogeneous ruthenium catalysts containing diazafluorene ligands *Appl. Organometal. Chem.* **30** 1030
30. Prasad K T, Therrien B and Kollipara M R 2008 Cationic half-sandwich complexes (Rh, Ir, Ru) containing 2-substituted-1,8-naphthyridine chelating ligands: Synthesis, X-ray structure analyses and spectroscopic studies *J. Organomet. Chem.* **693** 3049
31. Adhikari S, Hussain O, Phillips R M and Kollipara M R 2018 Half-sandwich d^6 metal complexes comprising of 2-substituted-1,8-napthyridine ligands with unexpected bonding modes: Synthesis, structural and anti-cancer studies *J. Organomet. Chem.* **854** 27
32. Adhikari S, Sutradhar D, Shepherd S L, Phillips R M, Chandra A K and Kollipara M R 2016 Neutral and cationic half-sandwich arene ruthenium, Cp*Rh and Cp*Ir oximato and oxime complexes: Synthesis, structural, DFT and biological studies *J. Organomet. Chem.* **820** 70
33. Gupta G, Park S, Lee S S and Kim J 2011 Syntheses and Molecular Structure of Dinuclear Transition Metal Complexes Bridged by Dipyridylamine Derivative Ligands *Z. Anorg. Allg. Chem.* **637** 1516
34. Tsolis T, Manos M J, Karkabounas S, Zelovitis I and Garoufis A 2014 Synthesis, X-ray structure determination, cytotoxicity and interactions with 9-methylguanine, of ruthenium (II) η^6-arene complexes *J. Organomet. Chem.* **768** 1
35. Govindaswamy P, Canivet J, Therrien B, Süss-Fink G, Stepnicka P and Ludvík J 2007 Mono and dinuclear rhodium, iridium and ruthenium complexes containing chelating 2,2'-bipyrimidine ligands: synthesis, molecular structure, electrochemistry and catalytic properties *J. Organomet. Chem.* **692** 3664
36. Tweedy B G 1964 Plant extracts with metal ions as potential antimicrobial agents *Phytopathology* **55** 910
37. Prabhakaran R, Geetha A, Thilagavathi M, Karvembu R, Krishnan V, Bertagnolli H and Natarajan K 2004 Synthesis, characterization, EXAFS investigation and antibacterial activities of new ruthenium (III) complexes containing tetradentate Schiff base *J. Inorg. Biochem.* **98** 2131
38. Ozsoy N, Candoken E and Akev N 2009 Implications for degenerative disorders: Antioxidative activity, total phenols, flavonoids, ascorbic acid, β-carotene and β-tocopherol in Aloe vera *Oxid. Med. Cell. Longev.* **2** 99